Modeling Electron Characteristics in an Ion Thruster Plume: Fully Kinetic PIC vs. Hybrid PIC

IEPC-2017-301

Presented at the 35th International Electric Propulsion Conference
Georgia Institute of Technology, Atlanta, Georgia, USA
October 8–12, 2017

Y. Hu * and J. Wang†
University of Southern California, Los Angeles, 90089, California, USA

Both fully kinetic Particle-in-Cell (PIC) and hybrid PIC simulations are carried out to investigate the emission of a collisionless, mesothermal plasma plume from an ion thruster. The hybrid PIC simulation adopts the commonly used assumption that the electrons may be modeled by the commonly used Boltzmann relation, while the fully kinetic PIC simulations are carried out using the real Xe^+ to electron mass ratio ($m_i/m_e = 241073.64$). The results show that both fully kinetic PIC and hybrid PIC lead to similar plume density structures but very different plume potentials. If one could ignore the ion and electron mixing region immediately downstream of the thruster, the main physics which is missing from a hybrid PIC plume model is that from the electron temperature change. Including the initial ion and electron mixing region further complicates the effects from the electrons. Since the electron characteristics in a plasma plume is non-equilibrium and anisotropic, neither the commonly used Boltzmann relation nor the more general polytropic relation is valid for modeling electrons in an ion thruster plume.

Nomenclature

$\mathbf{x}$, $\tilde{\mathbf{x}}$	= Coordinate vector (x, y, z) and its normalized expression
$\mathbf{v}$, $\tilde{\mathbf{v}}$	= Velocity vector (v_x, v_y, v_z) and its normalized expression
t, $\tilde{t}$	= Time and its normalized expression
ϵ_0	= Vacuum permittivity
e	= Elementary charge
k_b	= Boltzmann constant
γ	= Electron polytropic cooling coefficient
m_i, m_e	= Ion and electron mass
Φ, $\tilde{\Phi}$	= Electric potential and its normalized expression
n_i, $\tilde{n}_i$	= Ion number density and its normalized expression
n_e, $\tilde{n}_e$	= Electron number density and its normalized expression
λ_D	= Debye length
ω_{pi}, ω_{pe}	= Ion and electron plasma frequency
v_{ti}, v_{te}	= Ion and electron thermal velocity
C_s	= Ion acoustic velocity
v_{di}, $\tilde{v}_{di}$	= Ion drifting velocity and its normalized expression
v_{de}, $\tilde{v}_{de}$	= Electron drifting velocity and its normalized expression
v_{beam}, $\tilde{v}_{\text{beam}}$	= Beam velocity and its normalized expression

*yuanhu@usc.edu
†josephjw@usc.edu

Γ_i, Γ_e	= Ion and electron flux density
J_i, J_e	= Ion and electron current density
f_i, f_e	= Ion and electron flux velocity distribution function
$f_{i,M}$, $f_{e,M}$	= Ion and electron Maxwellian velocity distribution function
M_0	= Beam Mach number
$\tilde{L}_x$, $\tilde{L}_y$	= Normalized domain size in the x- and the y-direction
$\Delta\tilde{x}$, $\Delta\tilde{y}$	= Normalized mesh cell size in the x- and the y-direction
$\Delta\tilde{t}$	= Normalized simulation time step

I. Introduction

In an ion thruster, cold beam ions are emitted from the thruster exit to provide the thrust while thermal electrons are emitted from a neutralizer to neutralize the ion beam. Studies of ion thruster plume have mostly focused on the physics driven by ion dynamics. It is thought that the role of the electrons is to simply provide a charge neutralization mechanism. Hence, a common approach in plume studies is to assume that the electrons may be modeled as an equilibrium, massless fluid so to simplify the electron dynamics. This approach, combined with a further assumption that the electrons are isothermal, leads to the commonly used Boltzmann electron model that builds the relation relation between the electron density n_e and the potential Φ as:

$$n_e = n_0 \exp\left(\frac{e[\Phi - \Phi_0]}{k_b T_e}\right) \tag{1}$$

where k_b is the Boltzman constant, e is the elementary charge, T_e is the constant electron temperature in this model, n_0 and Φ_0 are the plasma density and potential at a reference state, respectively. Eq. (1) has been used in almost all electric propulsion plume studies so far. The standard plume simulation approach has been to use hybrid particle-in-cell (PIC), where the ions are treated as macro-particles and electrons are assumed to satisfy Eq. (1), seeing Refs.[1–3] and references therein. The isothermal condition can be relaxed by allowing T_e to change as a function of position in Eq. (1).[4,5] However, while the assumption that the electrons in a plasma plume may be modeled by the Boltzmann relation has been widely adopted, questions such as whether this assumption is valid or to what extent it is applicable have not been resolved.

As gas expansion in general is not an isothermal process, several studies have examined the isothermal assumption in Eq. (1). Refs.[6–10] examined the validity of the polytropic law given in Eq.(2) to model the electrons and investigated the electron cooling effects on plasma expansion,

$$\frac{T_e}{n_e^{\gamma-1}} = \frac{T_{e0}}{n_{e0}^{\gamma-1}} \tag{2}$$

where γ is the polytropic coefficient, T_{e0} and n_{e0} are the electron temperature and number density at the reference point. Note that $\gamma = 1$ corresponds to the Boltzmann relation Eq(1). For example, Merino and Ahedo[9] simulated the plasma expansion in a magnetic nozzle with a two-fluid model and observed that the electron cooling led to lower beam divergence. However, the exact cooling mechanisms were not identified, and hence the choice of γ was arbitrary in that study.[9]

A more fundamental question is whether the fluid model for electrons is valid at all. For a fluid electron model to be valid, the electrons need to be in a thermal equilibrium or near-equilibrium state. Based on kinetic theory, the random collisions between particles are the primary mechanism to reach the thermal dynamic equilibrium state. The long-range coulomb interaction in plasmas is generally not considered as an effective mechanism for equilibrium.[11] However, as the characteristic length scale in typical electric thruster plume problems is much less than the mean free path in the emitted plasma, particle-particle collisions are generally absent for electrons in the plasma plume. Refs.[12–15] applied fully kinetic PIC simulations, where both the ions and the electrons are treated as macro-particles, to study beam neutralization process. Hu and Wang[16,17] investigated the electron characteristics in a plasma plume. They found that the electrons in the plasma plume mostly undergo a non-equilibrium and anisotropic process. Neither the commonly used Boltzmann relation Eq. (1) nor the more general polytropic law Eq. (2) is a good assumption for modeling electrons in plasma plume.

This paper extends[16,17] and investigates the errors resulted from using the Boltzmann relation, Eq. (1), in a hybrid PIC simulation. In this study, both hybrid PIC simulation and fully kinetic PIC simulations

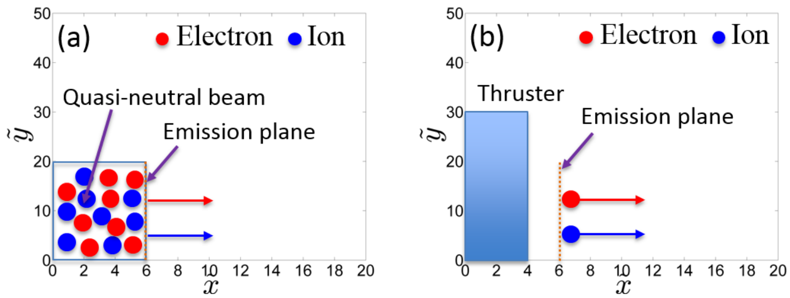

Figure 1. Schematics of different injection models: (a) quasi-neutral injection: Injection Setup 1; (b) current-free injection: Injection Setup 2.

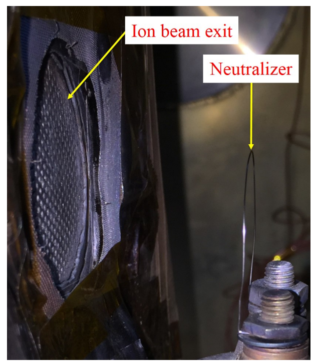

Figure 2. Photo of USC micro-ion thruster

using the actual Xe^+ ion to electron mass ratio are carried out. Section II describes the simulation model. Sections III and IV discuss the macroscopic plume property and microscopic electron kinetics, respectively. A summary and conclusions are presented in Section IV.

II. Simulation Approach and Models

In this study, we apply both fully kinetic and hybrid electrostatic (ES) particle-in-cell (PIC) simulations. In the fully kinetic PIC, both electrons and ions are modeled as particles. The dynamics of electrons and ions, the space charge, and the electric field are solved self-consistently from

$$\tilde{\nabla}^2\tilde{\Phi} = (\tilde{n}_e - \tilde{n}_i) \tag{3}$$

$$\frac{d}{d\tilde{t}}(\tilde{m}\tilde{\mathbf{v}}) = \tilde{\mathbf{F}}, \quad \tilde{\mathbf{v}} = \frac{d\tilde{\mathbf{x}}}{d\tilde{\mathbf{t}}} \tag{4}$$

where eqs.(3) and (4) are the normalized Poisson's equation and Newton's second law, respectively. In the hybrid PIC, only ions are treated as particles, and the electrons are assumed to follow the Boltzman relation given in Eq. (1). The electron density $\tilde{n}_e$ in Eq. 3 is replaced by Eq. (1).

The simulation variables are normalized by the parameters at the reference condition. However, the normalization schemes for the fully kinetic and the hybrid PIC are different. The fully kinetic PIC needs to resolve physics at the electron scale while the hybrid PIC only investigates the process at the ion time scale. Hence, the fully kinetic PIC uses dimensionless variables normalized by the electron plasma parameters, and the hybrid PIC uses those normalized by the ion plasma parameters. The normalization used for the fully kinetic PIC is as follows,

$$\tilde{\mathbf{x}} = \frac{\mathbf{x}}{\lambda_{D0}}, \quad \tilde{\mathbf{v}} = \frac{\mathbf{v}}{v_{te0}}, \quad \tilde{t} = t\omega_{pe0}, \quad \tilde{m}_{i,e} = \frac{m_{i,e}}{m_e}, \quad \tilde{n}_{i,e} = \frac{n_{i,e}}{n_0}, \quad \tilde{\Phi} = \frac{e\Phi}{k_bT_{e0}} \tag{5}$$

and the normalization for the hybrid PIC is given by,

$$\tilde{\mathbf{x}} = \frac{\mathbf{x}}{\lambda_{D0}}, \quad \tilde{\mathbf{v}} = \frac{\mathbf{v}}{C_{s0}}, \quad \tilde{t} = t\omega_{pi0}, \quad \tilde{m}_i = \frac{m_i}{m_i} = 1, \quad \tilde{n}_{i,e} = \frac{n_{i,e}}{n_0}, \quad \tilde{\Phi} = \frac{e\Phi}{k_b T_{e0}} \tag{6}$$

In Eqs. (5) and (6), the subscript "0" denotes the reference condition, $\lambda_{D0} = \sqrt{\epsilon_0 k_b T_{e0}/n_0 e^2}$ is the Debye length, $\omega_{pe0} = \sqrt{n_0 e^2/\epsilon_0 m_e}$ and $\omega_{pi0} = \sqrt{n_0 e^2/\epsilon_0 m_i}$ are the electron and the ion plasma frequency, respectively, $v_{te0} = \sqrt{k_b T_{e0}/m_e}$ is the electron thermal velocity, and $C_{s0} = \sqrt{k_b T_{e0}/m_i}$ is the ion acoustic velocity.

In an ion thruster, the beam emitted is current free but the region immediately next to the thruster exit and neutralizer is non-neutral. However, the hybrid PIC approach cannot resovle the ion beam neutralization process and thus only simulates a quasi-neutral plume. Hence, in this study we shall consider two different beam emission models, as illustrated in Fig. 1. The first one is the quasi-neutral beam injection setup (Injection Setup 1). In Injection Setup 1, we assume that a neutral plasma beam has already been formed within a reservoir upstream of the emission surface. Hence, the emission source is an equilibrium, well-neutralized plasma beam, where the ion and electron densities are equal ($n_{i0} = n_{e0}$), and the net current is balanced ($J_{i0} + J_{e0} = 0$). The fully kinetic PIC based approach allows the inclusion of the non-neutral beam region and the subsequent ion beam neutralization process. Hence, the second one is a non-quasi-neutral but current-free injection setup (Injection Setup 2). Here, we consider a plasma beam that is current-free, $J_{i0} + J_{e0} = 0$, but with a different initial number density, $n_{i0} \neq n_{e0}$.

Plasma thrusters may use a variety of neutralization designs. The Injection Setup 2 is similar to that of the USC micro-ion thruster which uses a thermionic emitter immersed in the ion beam for neutralization.[18] Fig. 2 shows the USC micro-ion thruster. In this source, ions are accelerated through an ion optics to form a cold beam with a directed energy of $\sim$ 1100eV. A hot-filament neutralizer is located downstream of the source exit inside the ion beam. Thermal electrons are emitted from the wire with a temperature of a few eV. The plasma beam immediately downstream of the emission surface is non-neutral.

The Injection Setup 1 is used in both the hybrid PIC and fully kinetic PIC simulations. In a fully kinetic PIC simulation, both the electrons and ions in the reservoir follow drifting Maxwellian distributions, and have the same drifting velocity as the beam velocity but very different thermal velocities.

$$f_{ie,M}(v_x) = \sqrt{\frac{m_{i,e}}{2\pi k_b T_{i,e0}}} \exp\left(-\frac{m_{i,e}[v_x - v_{\text{beam}}]^2}{2k_b T_{i,e0}}\right), \quad v_x \in (-\infty, \infty) \tag{7}$$

$$f_{ie,M}(v_y) = \sqrt{\frac{m_{i,e}}{2\pi k_b T_{i,e0}}} \exp\left(-\frac{m_{i,e} v_y^2}{2k_b T_{i,e0}}\right), \quad v_y \in (-\infty, \infty) \tag{8}$$

Note that we assume v_{beam} has only the x-component. At the emission surface, the ion flux density towards the simulation domain $\tilde{\Gamma}_i^+$ is much smaller than the electron flux density $\tilde{\Gamma}_e^+$ due to the difference of their thermal velocities. However, our recent fully kinetic simulation has shown that the emitted thermal electrons do have the ability to adjust themselves to keep a quasi-neutral, curren-free beam downstream of the emission source.[17] This quasi-neutral beam emission model naturally works for the hybrid PIC since the detailed electron kinetics are ignored and the electrons are assumed to reach equilibrium instantaneously in the hybrid PIC model.

The Injection Setup 2 was used only the fully kinetic PIC simulation. In Injection Setup 2, the simulation domain includes a fraction of the plasma source body. The emission surface is located a few λ_{D0} downstream of the source body.

The current-free condition for the emitted plasma, $J_i + J_e = 0$ or $\Gamma_i^+ = \Gamma_e^+$, is imposed at the emission surface. Because the electron's thermal velocity is much larger than the ion's, the current-free condition leads to a non-neutral plasma near the emission surface. However, a neutral beam can be formed downstream mainly because of the potential well established in the plume region, seeing Refs.[14,16,17] The x-component of the velocity of both the emitted ions and electrons is sampled from a flux velocity distribution by using an acceptance-rejection method described in.[19] The flux velocity distribution functions for the ion and the electron are given as follows,

$$f_{i,e}(v_x) = C_{i,e} v_x \exp\left(-\frac{m_{i,e}[v_x - v_{\text{beam}}]^2}{2k_b T_{i,e0}}\right), \quad v_x \geq 0 \tag{9}$$

where C_i and C_e are normalization factors such that the integral of $f_i(v_x)$ and $f_e(v_x)$ from 0 to ∞ equals 1. The y-component of the velocity for each species is sampled from the corresponding stationary Maxwellian velocity distribution function (Eq. (8)) with the Box-Muller method.

For a typical ion thruster, the radius of the plasma beam emitted, R_{beam}, is much larger than the Debye length at the emission source λ_{D0}. In the simulations, the size of the initial beam size in y is taken to be $R_{\text{beam}} = 20\lambda_{D0}$. As a result, we consider the beam reservoir is located in the region of $(\tilde{x}, \tilde{y}) = (0 \sim 6, 0 \sim 20)$ for the quasi-neutral injection model. Partiles are injected from the emission surface at $\tilde{x} = 6, \tilde{y} = 0 \sim 20$ according to the state of the neutral beam reservoir at each simulation step. The reservoir is kept Maxwellian and any particle that reaches the reservoir is absorbed immediately. The electric potential in the region of the reservoir is fixed at zero. For the current-free non-neutral injection model, the thruster body is set to occupy the region of $(\tilde{x}, \tilde{y}) = (0 \sim 4, 0 \sim 30)$, and its potential is fixed to be zero. The center of the plasma emission surface is the same as that for the quasi-neutral injection model, namely $\tilde{x} = 6, \tilde{y} = 0 \sim 20$. Particles that are attracted back to and eventually hit the thruster body are thermalized and re-injected into the simulation domain.

To speed up the computation, the simulation setups shown in Fig.1 were carried out in two-dimensions. Since xenon (Xe) is the most popular propellent for ion thrusters, we take the real Xe^+ ion to electron mass ratio $m_i/m_e = 241073.64$ for the fully kinetic PIC modeling in this study. The temperature ratio of ion to electron at the source exit is taken to be $T_{i0}/T_{e0} = 0.01$. We consider the Mach number of the beam to be $M_0 = v_{\text{beam}}/C_{s0} = 20$ for all the simulations in this paper. Accordingly, the beam velocity is set to be $v_{\text{beam}}/v_{te0} = 0.040734$.

The simulations need to run for a time duration long enough to achieve a steady state plume in the region near the thruster. The simulations also need to terminated far before the beam front reaches the boundary of simulation domain because it is difficult to accurately pre-determine the far field boundary condition for the fully kinetic PIC simulation of mesothermal plasma plume expansion. These two constrains determine the domain size and time in our simulation setup. The simulation domain used is $\tilde{L}_x \times \tilde{L}_y = 2000 \times 1000$, with a mesh size of $\Delta\tilde{x} = \Delta\tilde{y} = 1$. The symmetric boundary condition is applied at the plane of $\tilde{y} = 0$ for the field as well as the particles. The zero Neumann boundary condition for the electric field is applied at other boundaries of the simulation domain. The vacuum condition is used at the boundaries except the plane of $\tilde{y} = 0$ to absorb the particles (only thermal electrons) escaping the domain occasionally. The simulations are run for a time duration upto $t\omega_{pi0} = 35$. The time step used for the fully kinetic PIC simulation is $\Delta\tilde{t} = \Delta t\omega_{pe0} = 0.05$, and that for the hybrid PIC simulation is $\Delta\tilde{t} = \Delta t\omega_{pi0} = 0.01$. Note that $\omega_{pe0}/\omega_{pi0} = \sqrt{m_i/m_e} \simeq 491$ so the total simulation steps are 343700 for the fully kinetic PIC, and are 3500 for the hybrid PIC. We have checked the plume structures at the times of $t\omega_{pi0} = 25, 30$ and 35. The results show that at $t\omega_{pi0} = 30$, the plume reaches a steady state in the region of $\tilde{x} \leq 550$.

III. Results and Discussion

This section presents results using three different simulation models. Hereafter, we refer the hybrid PIC and the fully kinetic PIC simulations with the quasi-neutral beam injection model (Injection Setup 1, Fig. 1.a) as Simulation Model A and Simulation Model B, respectively, and refer the fully kinetic PIC modeling with the current-free injection model (Injection Setup 2, Fig. 1.b) as Simulation Model C. The hybrid PIC simulation assumes that the electrons follow the Boltzmann relation, Eq. (1). The fully kinetic PIC simulations are carried out for a Xe^+ plasma plume, using the real Xe^+ to electron mass ratio of $m_i/m_e = 241073.64$.

Fig. 3 shows the ion and electron number density contours obtained from the three simulation models. All three models show similar density distributions. In particular, although the beam is initially non-neutral at the emission surface in Model C, a well-neutralized beam is formed starting at about at about $3\lambda_{D0}$ downstream. The neutralization process for this emission setup was discussed in detail in Wang et al.[14] Figs. 4 and 5 further compare 1-D density profiles from the three simulation models along the beam direction and the transverse direction, respectively. Other than the noises shown in the fully kinetic PIC simulations far away from the emission surface (due to insufficient number of particles per cell), the fully kinetic PIC and the hybrid particle PIC provide the same result.

The expansion of a quasi-neutral mesothermal plasma into a vacuum has been studied both analytically and through hybrid PIC simulations. Wang and Hastings[20, 21] presented both analytical solution and hybrid PIC simulations using the Boltzmann electron model, Eq.(1), of the expansion of a mesothermal plasma flow

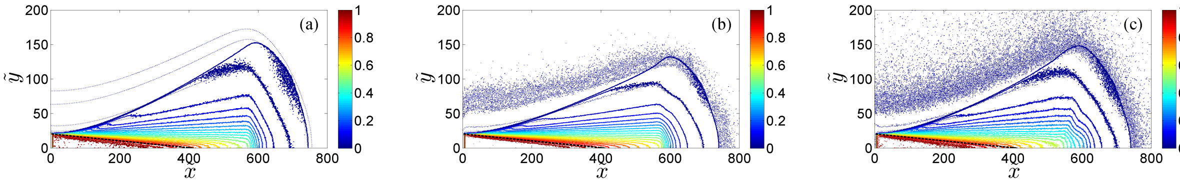

Figure 3. Number density contours for ions (colored "———") and electrons (colored "– · –") at $t\omega_{pi0} = 30$ ($t\omega_{pe0} \simeq 14730$). The black "– – –" represents the Mach line based on M_0 originating from the edge of the emission source, $(\tilde{x}_0, \tilde{z}_0) = (20, 6)$. Results of: (a) Model A, (b) Model B, and (c) Model C.

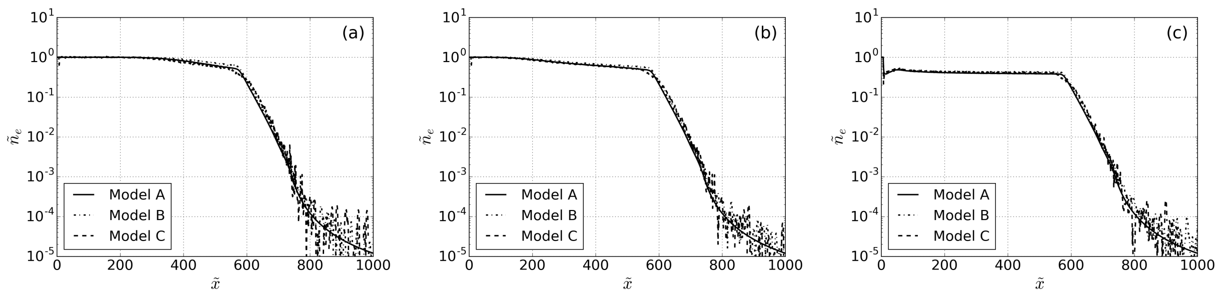

Figure 4. Density profiles along the beam direction (x-axis) of all the three models at $t\omega_{pi0} = 30$ ($t\omega_{pe0} \simeq 14730$): (a) $\tilde{y} = 0$, (b) $\tilde{y} = 10 (= 0.5\tilde{R}_{\text{beam}})$ (c) $\tilde{y} = 20 (= \tilde{R}_{\text{beam}})$.

into the wake of a large plate. In a quasi-neutral meosthermal plasma flow expansion, the boundary that separates the undisturbed plasma flow from the expansion region would be the first characteristic line of the expansion fan, which is also the Mach line computed based on the Mach number inside the undisturbed region.[20,21] The relation between the slope of the Mach line and the the Mach number is

$$k = \tan(\theta), \quad \text{where } \theta \simeq \sin^{-1}\left(\frac{1}{M_0}\right) \tag{10}$$

In Fig.3, the black dashed line is the Mach line intersecting the edge of the source exit, computed using the Mach number at the emission exit, M_0. In the simulation, the inner expansion boundary qualitatively agrees with this result.

Fig. 6 compares the potential contours obtained from the three simulation models. While the density contours are similar from all three models, there are significant differences in the potential contours between

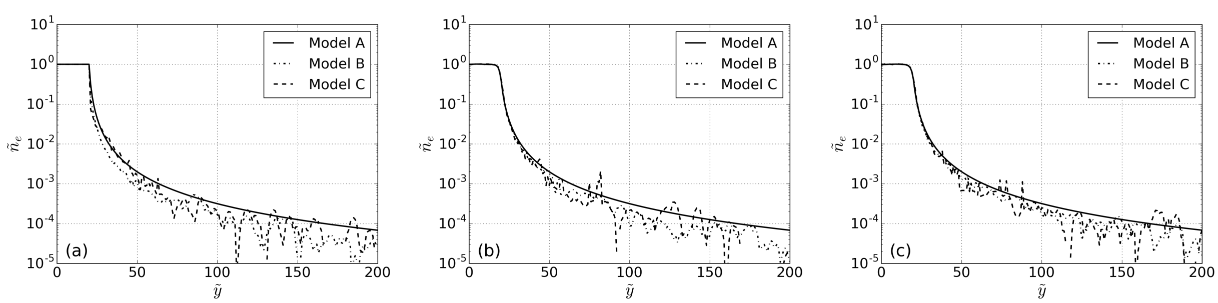

Figure 5. Density profiles along the transverse direction (y-axis) of all the three models at $t\omega_{pi0} = 30$ ($t\omega_{pe0} \simeq 14730$): (a) $\tilde{x} - \tilde{x}_{\text{emission plane}} = 0$, (b) $\tilde{x} - \tilde{x}_{\text{emission plane}} = 10 (= 0.5\tilde{R}_{\text{beam}})$, (c) $\tilde{x} - \tilde{x}_{\text{emission plane}} = 20 (= \tilde{R}_{\text{beam}})$.

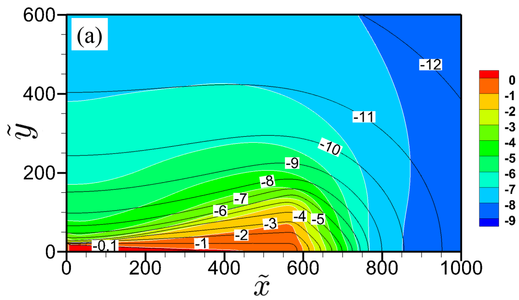

Figure 6. Comparisons of potential contours between fully kinetic PIC and hybrid PIC results at $t\omega_{pi0} = 30$ ($t\omega_{pe0} \simeq 14730$): (a) Model B versus Model A, (b) Model C versus Model A. The fully kinetic PIC results (Model B and Model C) are shown by colored contours. The hybrid PIC result (Model A) is shown as black contour lines with valued labels and laid out together with the fully kinetic PIC results.

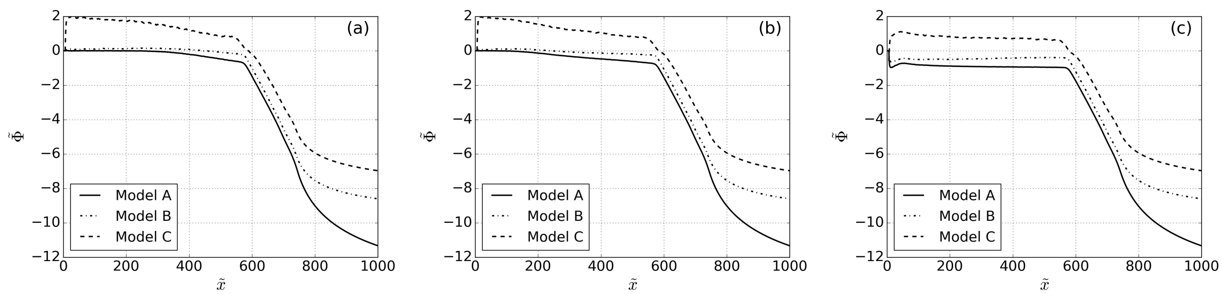

Figure 7. Potential profiles along the beam direction (x-axis) of all the three models at $t\omega_{pi0} = 30$ ($t\omega_{pe0} \simeq 14730$): (a) $\tilde{y} = 0$, (b) $\tilde{y} = 10 (= 0.5\tilde{R}_{\mathrm{beam}})$ (c) $\tilde{y} = 20 (= \tilde{R}_{\mathrm{beam}})$.

the hybrid PIC and the fully kinetic PIC. For both Injection Setup 1 and Setup 2, the hybrid PIC simulation (Model A) shows a significant higher potential difference from the plume to the ambient. Figs. 7 and 8 further compare 1-D potential profiles from the three simulation models along the beam direction and the transverse direction, respectively. These profiles show that the hybrid PIC approach leads to significantly larger potential drop from the plume center to ambient.

The discrepancy between the hybrid PIC and fully kinetic PIC is to be expected. The assumption of the Boltzmann relation Eq. (1) ignores both macroscopic energy transfer and microscopic kinetic processes of the electrons. From Eq. (1) and allows an infinitely large potential drop as the electron density decreases. This is clearly an unphysical result. It is also not surprising that the density profiles obtained from Model A are similar to Models B and C. This is because the potential drop in the plume is small as compared to the kinetic energy of the beam ions to have any noticeable effects on the beam ion trajectories and density distribution. The electron density distribution follows the ion density distribution. Hence, the effect of the

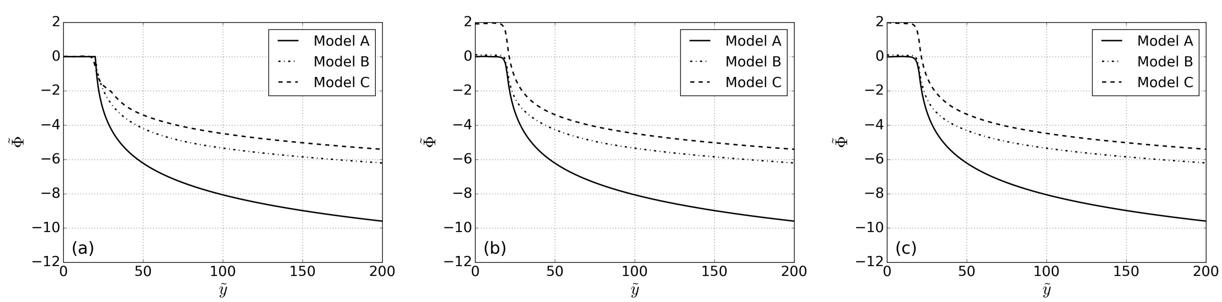

Figure 8. Potential profiles along the transverse direction (y-axis) of all the three models at $t\omega_{pi0} = 30$ ($t\omega_{pe0} \simeq 14730$): (a) $\tilde{x} - \tilde{x}_{\mathrm{emission\ plane}} = 0$, (b) $\tilde{x} - \tilde{x}_{\mathrm{emission\ plane}} = 10 (= 0.5\tilde{R}_{\mathrm{beam}})$, (c) $\tilde{x} - \tilde{x}_{\mathrm{emission\ plane}} = 20 (= \tilde{R}_{\mathrm{beam}})$.

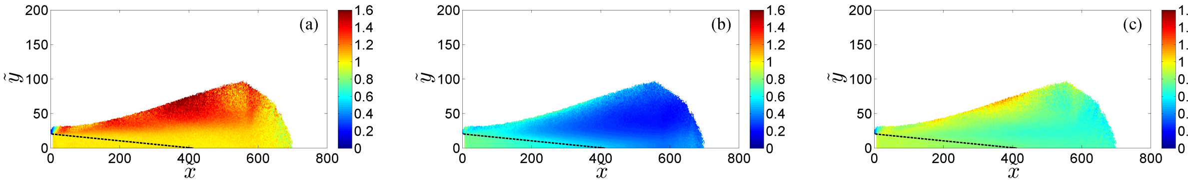

Figure 9. Contours of electron temperature predicted by Model B at $t\omega_{pi0} = 30$ ($t\omega_{pe0} \simeq 14730$). The black "— — —" represents the Mach line based on M_0 originating from the edge of the emission source, $(\tilde{x}_0, \tilde{z}_0) = (20, 6)$. Results of: (a) $\gamma(\tilde{T}_{e,x})$, (b) $\gamma(\tilde{T}_{e,y})$, (c) $\gamma(\tilde{T}_{e,\text{avg}})$.

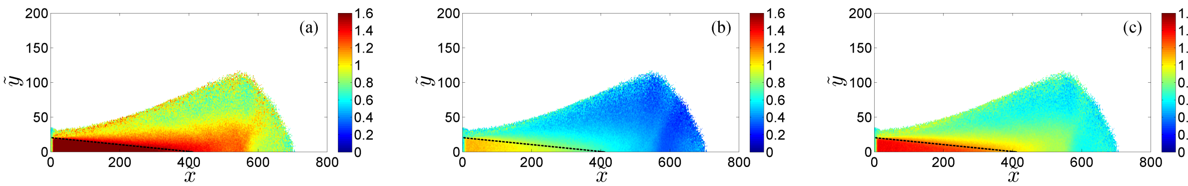

Figure 10. Contours of electron temperature predicted by Model C at $t\omega_{pi0} = 30$ ($t\omega_{pe0} \simeq 14730$). The black "— — —" represents the Mach line based on M_0 originating from the edge of the emission source, $(\tilde{x}_0, \tilde{z}_0) = (20, 6)$. Results of: (a) $\gamma(\tilde{T}_{e,x})$, (b) $\gamma(\tilde{T}_{e,y})$, (c) $\gamma(\tilde{T}_{e,\text{avg}})$.

discrepancy in plume potential on plume density distribution is minimum.

The effects of microscopic electron characteristics on macroscopic plume properties are most easily observed through electron temperature in the plume. Figs. 9 and 10 show the contours of the electron temperature obtained from Model B and Model C, respectively. The electron temperature $\tilde{T}_e$ refers to the second electron velocity moment averaged over the macro-particles within each cell. The normalized 2-D electron temperature at each mesh point is calculated from

$$\tilde{T}_{e,j}(\tilde{x}, \tilde{y}) = \tilde{v}^2_{te,j}(\tilde{x}, \tilde{y}) = (< \tilde{v}^2_j > - < \tilde{v}_j >^2) \tag{11}$$

Here, $j = x, y$ refers to the electrons' motion in the corresponding direction, and $< \cdot >$ indicates a quantity averaged over individual particles within each cell.

$$< \tilde{v}^n_j >= \sum_{p=1}^{N_p} \tilde{v}^n_p(j)/N_p \tag{12}$$

where $n = 1, 2$ and N_p is the number of macro-particles in a given cell. The statistical noise of $\tilde{T}_{e,j}$ in each cell is $\text{std}((\tilde{v}_j - < \tilde{v}_j >)^2)/\sqrt{N_p}$, where std is the standard deviation. To reduce the interference of the statistical noise, the calculation of eq(11) was carried out only for those cells with a number of macro-particles per cell $N_p \geq 16$. We also take the average temperature into consideration.

$$\tilde{T}_{e,\text{avg}} = \left(\tilde{T}_{e,x} + \tilde{T}_{e,y}\right)/2 \tag{13}$$

Considering that the electron temperature is highly anisotropic, we may need to investigate the polytropic relation for the electron temperature in different directions. According to the polytropic relation given in Eq. (2), we can write the polytropic coefficients for different components of the electron temperature as,

$$\gamma(\tilde{T}_{e,j}) = 1 + \frac{\log(\tilde{T}_{e,j}/\tilde{T}_{e0})}{\log(\tilde{n}_e/\tilde{n}_{e0})} \tag{14}$$

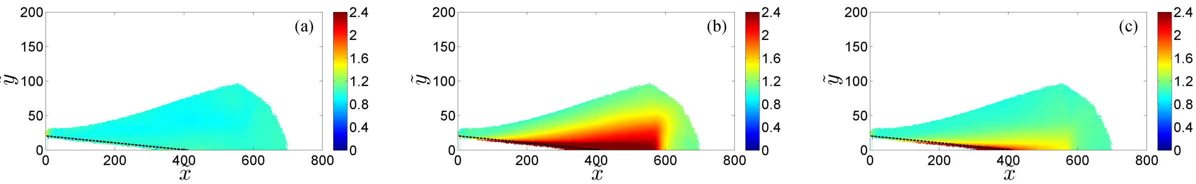

Figure 11. Contours of polytropic coefficient γ predicted by Model B at $t\omega_{pi0} = 30$ ($t\omega_{pe0} \simeq 14730$). The black "— — —" represents the Mach line based on M_0 originating from the edge of the emission source, $(\tilde{x}_0, \tilde{z}_0) = (20, 6)$. Results of: (a) $\gamma(\tilde{T}_{e,x})$, (b) $\gamma(\tilde{T}_{e,y})$, (c) $\gamma(\tilde{T}_{e,\text{avg}})$.

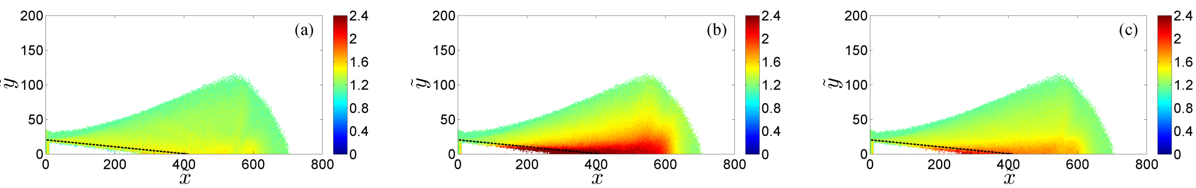

Figure 12. Contours of polytropic coefficient γ predicted by Model C at $t\omega_{pi0} = 30$ ($t\omega_{pe0} \simeq 14730$). The black "— — —" represents the Mach line based on M_0 originating from the edge of the emission source, $(\tilde{x}_0, \tilde{z}_0) = (20, 6)$. Results of: (a) $\gamma(\tilde{T}_{e,x})$, (b) $\gamma(\tilde{T}_{e,y})$, (c) $\gamma(\tilde{T}_{e,\text{avg}})$.

where $\tilde{T}_{e,j} = \tilde{T}_{e,x}$, $\tilde{T}_{e,y}$ or $\tilde{T}_{e,\text{avg}}$. Figs. 11 and 12 also show contours of the polytropic coefficient γ obtained from Model B and Model C, respectively.

The electron temperature T_e contours from Model B show that $T_{e,x}$ and $T_{e,y}$ behave very different. The conotour of $T_{e,y}$ shows mostly electron cooling as the plume expands outward, as expected. However, $T_{e,x}$ is a relative constant inside the main beam region but exhibits a slight heating in the plume expansion region. The polytropic coefficient γ contours from Model B show that the γ for $T_{e,x}$ is $\gamma \sim 0.9$ in the plume expansion region and is $\gamma \sim 1$ inside the beam region, consistent with the $T_{e,x}$ contours.

The electron temperature T_e contours from Model C exhibit a more complex behavior. The main difference from the result of Model B is that there is also a heating region for $T_{e,x}$ inside the main beam. This is due to electron acceleration by the sheath next to the emission surface. Ref.[17] also studied the T_e characteristics using Model C for a proton plasma plume and observed the similar behavior. Hence, the initial ion electron mixing region will have a significant influence on the electron characteristics in the plume. (see Ref.[17] for more detailed discussion on the influence of the ion electron mixing region on microscopic electron characteristics). The polytropic contours of γ for $T_{e,y}$ from both Model B and Model C show that the γ ranges from 1.2 to 2.4.

IV. Conclusion

Both hybrid PIC and fully kinetic PIC simulations were carried out to investigate the emission of a collisionless, mesothermal plasma plume. The hybrid PIC simulation adopted the commonly used assumption that the electrons may be modeled using the Boltzmann relation, Eq. (1). The fully kinetic PIC simulations were carried out using the real Xe^+ to electron mass ratio ($m_i/m_e = 241073.64$). The focus is on the electron characteristics and the validity of the commonly used Boltzmann relation for electrons in plume modeling.

Three different simulations were carried out. Simulation Model A and Model B considered the emission of a beam that was already completely neutralized upstream of the emission surface (Injection Setup 1) using hybrid PIC and fully kinetic PIC, respectively. Simulation Model C considered the emission of a current-free but initially non-neutralized beam (Injection Setup 2) using fully kinetic PIC. In Simulation Model C, beam neutralization was achieved self-consistently in the simulation.

The results show that all three models lead to similar plume density structures but very different plume potentials. If one could exclude the ion and electron mixing region immediately downstream of the thruster, the main physics that is missing from a hybrid PIC plume modeling that from electron temperature change. Since the initial ion-electron mixing region drives the ion beam neutralization process, and thus has a significant effect on electron microscopic kinetic characteristic, including the initial ion and electron mixing region further complicates the effects from the electrons. Since the electron characteristics in a plasma plume is non-equilibrium and anisotropic, neither the commonly used Boltzmann relation, Eq. (1), nor the more general polytropic relation, Eq. (2) is valid for modeling electrons in a plasma plume. This paper considered electrons emitted from a neutralizer immersed in the ion beam. Future studies will need to resolve the physics in the ion-electron mixing region for more complex neutralization schemes.

Acknowledgments

We acknowledge computational resources provided by the Center for High Performance Computing at the University of Southern California.

References

[1] J Wang, D Brinza, and M Young. Three-dimensional particle simulations of ion propulsion plasma environment for deep space 1. *J. Spacecraft and Rockets*, 38(3):433–440, May-Jun 2001.

[2] ID Boyd. Review of hall thruster plume modeling. *J. Spacecraft and Rockets*, 38(3):381–387, May-Jun 2001.

[3] Joseph Wang, Yong Cao, Raed Kafafy, Julien Pierru, and Viktor Decyk. Simulations of ion thruster plume spacecraft interactions on parallel supercomputers. *IEEE Trans. Plasma Sci.*, 34(5):2148–2158, Oct 2006.

[4] RIS Roy, DE Hastings, and NA Gatsonis. Ion-thruster plume modeling for backflow contamination. *J. Spacecraft and Rockets*, 33(4):525–534, Jul-Aug 1996.

[5] N A Gatsonis and X Yin. Hybrid (particle/fluid) modeling of pulsed plasma thruster plumes. *Journal of Propulsion and Power*, 17(5):945–958, Sept-Oct 2001.

[6] J Denavit. Collisionless plasma expansion into a vacuum. *Phys. Fluids*, 22(7):1384–1392, 1979.

[7] P Mora and R Pellat. Self-similar expansion of a plasma into a vacuum. *Phys. Fluids*, 22(12):2300–2304, 1979.

[8] G Manfredi, S Mola, and MR Feix. Rescaling methods and plasma expansions into vacuum. *Phys. Fluids B-Plasma Phys.*, 5(2):388–401, Feb 1993.

[9] M Merino and E Ahedo. Influence of electron and ion thermodynamics on the magnetic nozzle plasma expansion. In *The 33rd International Electric Propulsion Conference*, number IEPC-2013-247, The George Washington University, Washington, D.C., USA, Oct 2013.

[10] M. Martinez-Sanchez, J. Navarro-Cavalle, and E. Ahedo. Electron cooling and finite potential drop in a magnetized plasma expansion. *Phys. Plasmas*, 22:053501, 2015.

[11] E.M. Lifshitz and L.P. Pitaevskii. *Physical Kinetics*, volume 10 of *Course of Theoretical Physics*, chapter 3. Butterworth-Heinemann, 1 edition, Dec 1976.

[12] A Wheelock, D Cooke, and N A Gatsonis. Investigation of ion beam neutralization processes with 2-d and 3-d pic simulations. *Comput. Phys. Comm.*, 164:336–343, 2004.

[13] Lubos Brieda and Joseph Wang. Modeling of ion thruster beam neutralization using a fully kinetic es-pic code. In *AIAA*, number 2005-4045, Tucson, Arizona, USA, July 2005.

[14] Joseph Wang, Ouliang Chang, and Yong Cao. Electron-ion coupling in mesothermal plasma beam emission: Full particle pic simulations. *IEEE Trans. Plasma Sci.*, 40(2):230–236, Feb 2012.

[15] H. Usui, A. Hashimoto, and Y. Miyake. Electron behavior in ion beam neutralization in electric propulsion: full particle-in-cell simulation. *Journal of Physics: Conference Series*, 454:012017, 2013.

[16] Yuan Hu and Joseph Wang. Electron properties in collisionless mesothermal plasma expansion: Fully kinetic simulation. *IEEE Trans. Plasma Sci.*, 43(9):2832–2838, Sep 2015.

[17] Yuan Hu and Joseph Wang. Fully kinetic simulations of collisionless, mesothermal plasma emission: Macroscopic plume structure and microscopic electron characteristics. *Physics of Plasmas*, 24(3):033510, 2017.

[18] J Polansky, J Wang, and N Ding. Experimental investigation on plasma plume potential. *IEEE Trans. Plasma Sci.*, 41(12):3438–3447, Dec 2013.

[19] G.A. Bird. *Molecular Gas Dynamics and the Direct Simulation of Gas Flows*, chapter 12. Clarendon Press, 2 edition, 1994.

[20] J Wang and DE Hastings. Ionospheric plasma flow over large high-voltage space platforms. i: Ion-plasma-time scale interactions of a plate at a zero-angle of attack. *Phys. Fluids B-Plasma Phys.*, 4(6):1597–1614, Jun 1992.

[21] J Wang and DE Hastings. Ionospheric plasma flow over large high-voltage space platforms. ii: The formation and structure of plasma wake. *Phys. Fluids B-Plasma Phys.*, 4(6):1615–1629, Jun 1992.